https://doi.org/10.37434/tpwj2021.01.04

COMPARATIVE ANALYSIS OF THE RESULTS OF COMPUTER SIMULATION OF HEAT TRANSFER AND HYDRODYNAMIC PROCESSES IN THE METAL BEING WELDED BY MEANS OF DIFFERENT SOFTWARE TOOLS

O.P. Semenov[1], **I.V. Krivtsun**[1], **A.V. Lykhoshva**[1], **O.I. Hluchenkyi**[2] and **O.I. Bondar**[2]
[1]E.O. Paton Electric Welding Institute of NAS of Ukraine,
11 Kazymyr Malevych Str., 03150, Kyiv, Ukraine. E-mail: office@paton.kiev.ua
[2]The Institute of Electrodynamics of NAS of Ukraine
56 Peremohy Prosp. 03057, Kyiv, Ukraine

In this work we considered two software tools for the purpose of multiphysics simulation of physical phenomena in weld pool: COMSOL Multiphysics and in-hose finite element (FE) code implemented in Wolfram Mathematica. For validation purpose, two test problems dealing with Marangoni induced convection are solved. Good agreement between benchmark solutions and obtained results is observed. Developed numerical algorithms and computer code can readily be employed for multiphysics simulation in welding. 14 Ref., 1 Table, 8 Figures.

Keywords: marangoni convection, weld pool shape, mathematical modelling, laser beam welding

Convection is the main mechanism of heat transfer in the weld pool during fusion welding and it significantly influences on final penetration of the weld. The driving forces for fluid flow in the weld pool include buoyancy force, electromagnetic force, the shear stress induced by surface tension gradient (Marangoni effect) on the free surface and mechanical interaction with arc plasma [1, 2]. While Lorentz force appears only in arc welding, Marangoni induced convection inherent to all types of fusion welding. By means of methods of physical simulation it was shown that Marangoni force gives rise to appearance of two counter rotating cells in meridional section of the weld pool in the case of spot welding [3]. Simulations performed in [4] confirm suchlike flow pattern. However, surface tension is highly effected by presence of surfactants and non-monotonically depends on temperature [5, 6] that is eventually influences on penetration depth [7]. That fact significantly complicates experimental determination of surface tension of liquid metals in conditions inherent to fusion welding. Influence of Lorentz force on convection in TIG welding is determined by welding current and dimension of anode region. The smaller the anode spot the greater the Lorentz force pushes the liquid metal downward [8, 9], and thereby increasing pool depth. Detailed experimental investigation of each driven force separately deals with considerable technical difficulties. Therefore, methods of Computational Fluid Dynamics (CFD) nowadays remain the most popular tools for the analysis of the coupled physical processes in the weld pool. A lot of possibilities exist to simulate heat transfer, electromagnetic and hydrodynamic processes in the weld pool. However, simulation results obtained by different software tools may differ. Careful verification should proceed the complex multiphysics simulation of the above mentioned phenomena. In current paper we focus on comparative analysis of simulation results of heat and mass transfer processes in weld pool obtained separately by commercial software COMSOL Multiphysics and in-hose FE code. For validation of algorithms and computer codes, we considered two numerical test cases, which are concerned with thermocapillary flow.

Governing equations. Model of hydrodynamic processes is based on Navier-Stokes equations for incompressible fluid, which in the case of axial symmetry can be written as follows

$$\rho\left(\frac{\partial u}{\partial t}+u\frac{\partial u}{\partial r}+v\frac{\partial u}{\partial z}\right)=\frac{1}{r}\frac{\partial}{\partial r}\left(r\sigma_{rr}\right)+\frac{\partial \sigma_{rz}}{\partial z}- \\ -\frac{\sigma_{\phi\phi}}{r}-u\frac{C\left(1-f_l\right)^2}{f_l^3+e_0}; \quad (1)$$

I.V. Krivtsun – https://orcid.org/0000-0001-9818-3383

$$\rho\left(\frac{\partial v}{\partial t}+u\frac{\partial v}{\partial r}+v\frac{\partial v}{\partial z}\right)=\frac{1}{r}\frac{\partial}{\partial r}\left(r\sigma_{rz}\right)+ \\ +\frac{\partial\sigma_{zz}}{\partial z}-v\frac{C\left(1-f_l\right)^2}{f_l^3+e_0}; \quad (2)$$

$$\frac{1}{r}\frac{\partial}{\partial r}\left(ru\right)+\frac{\partial v}{\partial z}=0. \quad (3)$$

Here r, z are the radial and axial coordinates accordingly, u, v, P are the velocity components and pressure respectively, ρ denote density of the fluid, σ_{rr}, σ_{zz}, σ_{rz}, $\sigma_{\phi\phi}$ are the nonzero components of stress tensor. For Newtonian fluid we have relations

$$\sigma_{rr}=-P+2\mu\frac{\partial u}{\partial r},\ \sigma_{zz}=-P+2\mu\frac{\partial v}{\partial z},\ \sigma_{rz}= \\ =\mu\left(\frac{\partial u}{\partial z}+\frac{\partial v}{\partial r}\right),\ \sigma_{\phi\phi}=-P+2\mu\frac{u}{r}. \quad (4)$$

where μ is dynamic viscosity. Last two terms in the right-hand sides of equations (1), (2) describe fluid deceleration in the mushy zone [10]. Here f_l is a liquid fraction, C is a constant of mushy region, e_0 is a small value constant which prevents division by zero. In solid region these terms totally dominate all the terms in the momentum equations so that velocity vanishes. For description of heat transfer processes we employ energy conservation equation written in enthalpy form

$$\rho\left(\frac{\partial h}{\partial t}+u\frac{\partial h}{\partial r}+v\frac{\partial h}{\partial z}\right)= \\ =\frac{1}{r}\frac{\partial}{\partial r}\left(r\lambda\frac{\partial T}{\partial r}\right)+\frac{\partial}{\partial z}\left(\lambda\frac{\partial T}{\partial z}\right), \quad (5)$$

where λ is thermal conductivity, h and T denote specific enthalpy and temperature, which in turn are related by

$$h\left(T\right)=\int_{T_0}^{T}c\left(\tilde{T}\right)d\tilde{T}+Lf_l\left(\tilde{T}\right). \quad (6)$$

Variables c and L in (6) denote specific heat and latent heat of fusion accordingly, T_0 is initial temperature of material. Finally, the liqi d fraction temperature dependence is chosen by the next way

$$f_l\left(T\right)=\begin{cases}0, & T<T_s\\ (T-T_s)/(T_l-T_s), & T_s\le T\le T_l,\\ 1, & T>T_l\end{cases} \quad (7)$$

where T_s, T_l are the solidus and liqi dus temperatures respectively. Governing eqa tions are solved numerically by means of characteristic-based finite element method [11]. We use qa drilaterals elements along with linear shape functions for pressure approximation and qa dratic one for temperature and velocity fields. All the numerical algorithms were implemented in Wolfram Language.

Test problem 1. Marangoni convection in a thin liquid layer. The first test problem presented is a plane Marangoni convection in a thin liquid layer with infinite length (Figure 1). Phase change effects are not included in the model. By assumption the surface tension is quadratically dependent on temperature by $\sigma = \sigma_0 + \alpha(T - T_c)^2/2$, where σ_0, α are the constant values and T_c is a critical temperature at which surface tension reaches a minimum. Boundary conditions to the problem considered are the next

$$y=0,\ u=v=0,\ T=T_c+Ax \quad (8)$$

$$y=H,\ \mu\frac{\partial u}{\partial y}=\frac{d\sigma}{dT}\frac{\partial T}{\partial x},\ v=0,\ \frac{\partial T}{\partial y}=0, \quad (9)$$

where A = const, H is a layer thickness. The first condition from (9) reflects the balance of thermocapillary force and shear stress on the free surface. An analytical solution of this problem was derived in [12] for small Marangoni number, defined by $Ma = \alpha A^2H^3\rho/\mu^2$. The space coordinates, velocities are made dimensionless by H and $\mu Ma/(H\rho)$ respectively. The temperature is nondimensionalized as $(T - T_c)/(AH)$. For the numerical analysis we chose finite computation region with aspect ratio 1/20. Calculation were carried out by means of in-hose code. Because of sign change in surface tension temperature gradient $\gamma = d\sigma/dT$ at $x = 0$, flow pattern has a symmetrical structure (Figure 1). A good agreement with benchmark solution is observed under $Ma = 1$ (Figure 2). In the case of high Ma numbers the discrepancy between analytical and numerical solutions becomes significant.

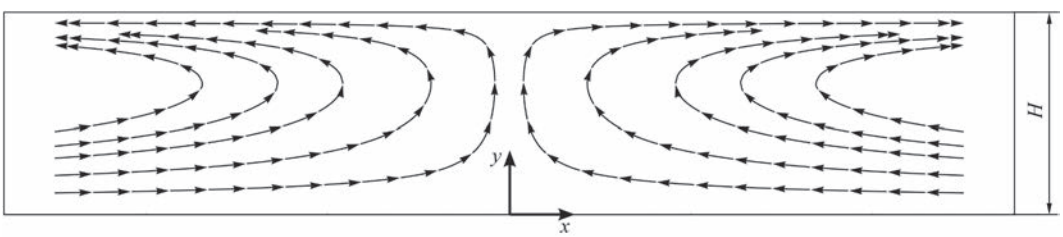

Figure 1. Thermocapillary convection in a thin liqi d layer

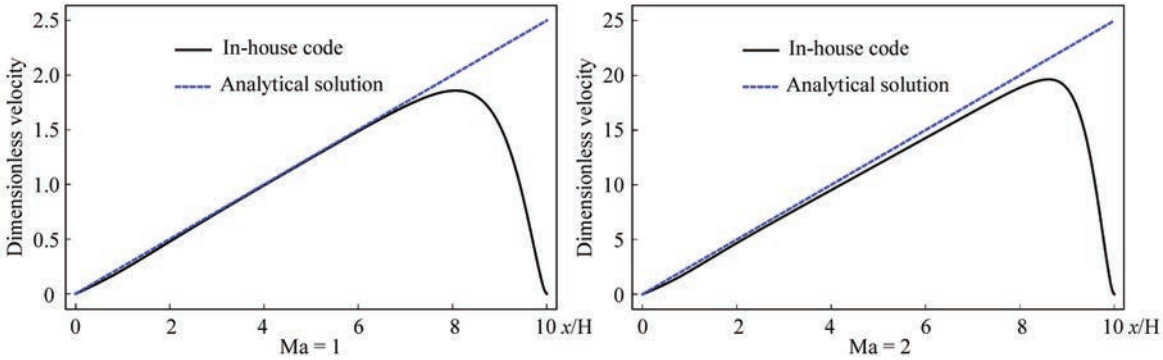

Figure 2. Velocity distribution along free surface of the liquid layer

Test problem 2. Marangoni induced convection in weld pool during laser spot welding. The problem considered in [13] dealing with weld pool dynamics in laser spot welding of the Böhler S705 steel was selected as a second benchmark problem. In paper [14] the same problem was considered. Open source finite volume CFD code OpenFoam was used in work [13] whereas in-house code Argo DG based on FEM was utilized in [14] for calculations. All the physical processes considered are supposed to be axisymmetric. Both thermocapillary and phase change effects are included in the model. Guided by the papers [13, 7] the values of liquid thermal conductivity and dynamic viscosity were increased by a factor of 7. Such an approach aimed at accounting for the enhanced heat and mass transfer caused by the development of hydrodynamic instabilities in the melt. In addition, coefficient γ is supposed to depend on temperature and sulfur content in the metal (Figure 3). Theoretical approach proposed in [5] was used for its description. Boundary conditions to the problem are the next:

$$\mu \left.\frac{\partial u}{\partial r}\right|_{CD} = \left.\frac{d\sigma}{dT}\frac{\partial T}{\partial r}\right|_{CD}; \quad (10)$$

$$v|_{CD} = u|_{AB} = v|_{AB} = u|_{BC} = v|_{BC} = u|_{AD} = 0; \quad (11)$$

$$\lambda \left.\frac{\partial T}{\partial z}\right|_{CD} = \begin{cases} \dfrac{\eta Q}{\pi r_q^2}, r \le r_q \\ 0, r > r_q \end{cases}; \quad (12)$$

$$\left.\frac{\partial T}{\partial z}\right|_{AB} = \left.\frac{\partial T}{\partial r}\right|_{BC} = \left.\frac{\partial T}{\partial r}\right|_{AD} = 0. \quad (13)$$

Here Q, r_q are the laser power and beam radius respectively, η is the absorptivity coefficient. Computation region is a cylinder of radius L_r = 15 mm and of height L_z = 15 mm (Figure 4). Physical properties of the material and heat source parameters are summarized in Table 1. Constants appeared in momentum sink terms were chosen as $e_0 = 10^{-3}$ and $C = 10^6$. Phase change was assumed to occur in the temperature interval from $T_s = T_m - 25$K to $T_l = T_m + 25$K. It was also supposed that sulfur concentration in metal is 20 ppm.

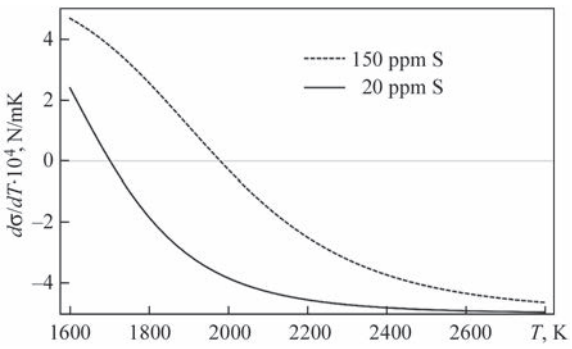

Figure 3. Surface tension temperature gradient for different sulfur contents

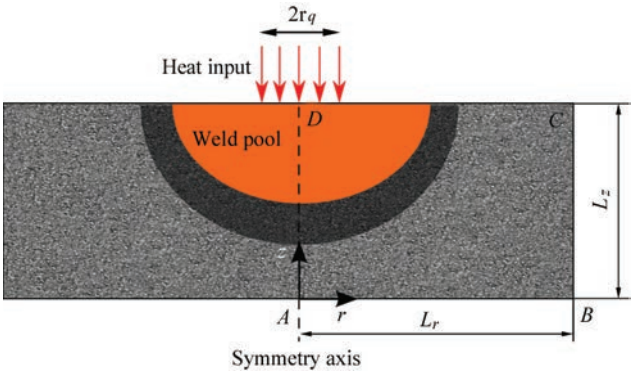

Figure 4. Computational domain

Properties of the Böhler S705 steel and laser beam settings

Density ρ, kg·m^{-3}	7200
Melting temperature T_m, K	1620
Dynamic viscosity μ, Pa·s	$6 \cdot 10^{-3}$
Heat capacity of liquid c_l, J·(kg·K)$^{-1}$	723.14
Heat capacity of solid c_s, J·(kg K)$^{-1}$	627
Thermal conductivity of solid λ_s, W/mK	22.9
Thermal conductivity of liquid λ_l, W/mK	22.9
Latent heat of fusion L, J·kg^{-1}	$2.508 \cdot 10^5$
Power of heat source Q, kW	5.2
Laser beam radius r_q, mm	1.4
Laser absorptivity η	0.13
Enhancement factor f,	7

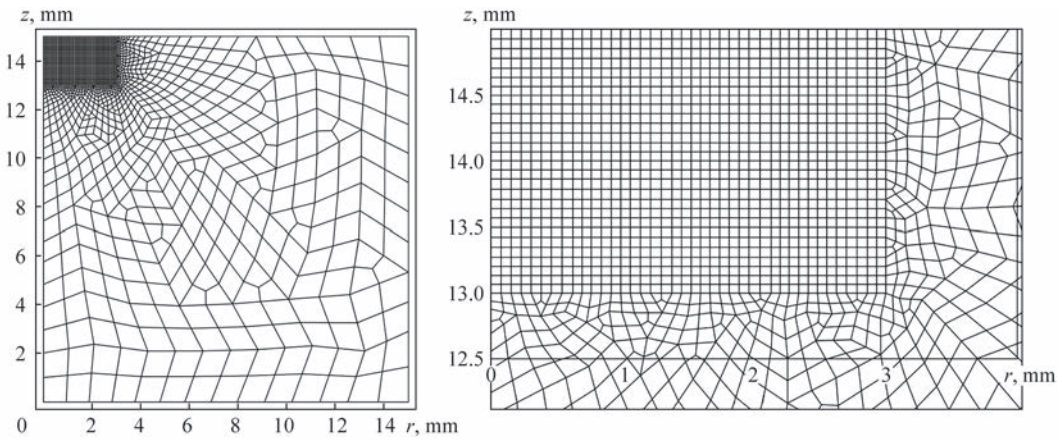

Figure 5. Adaptive finite element tessellation of computational domain

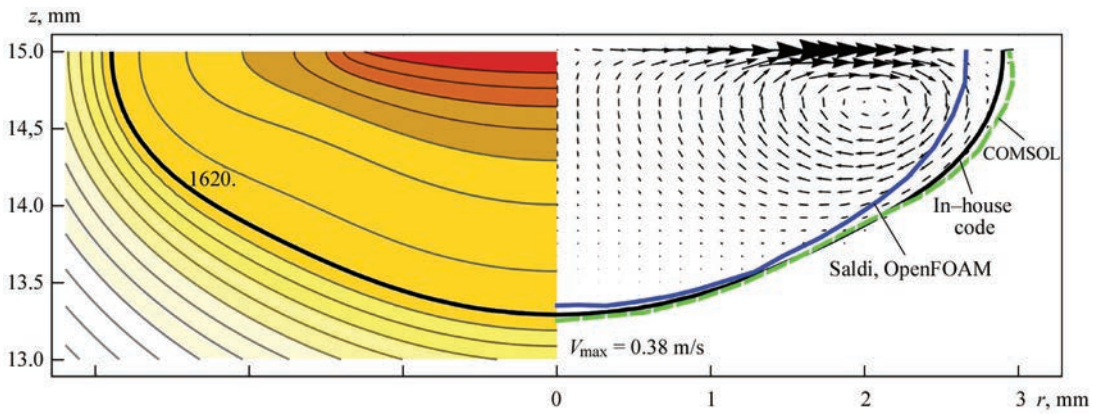

Figure 6. Melting front position and velocity field at t = 5 s

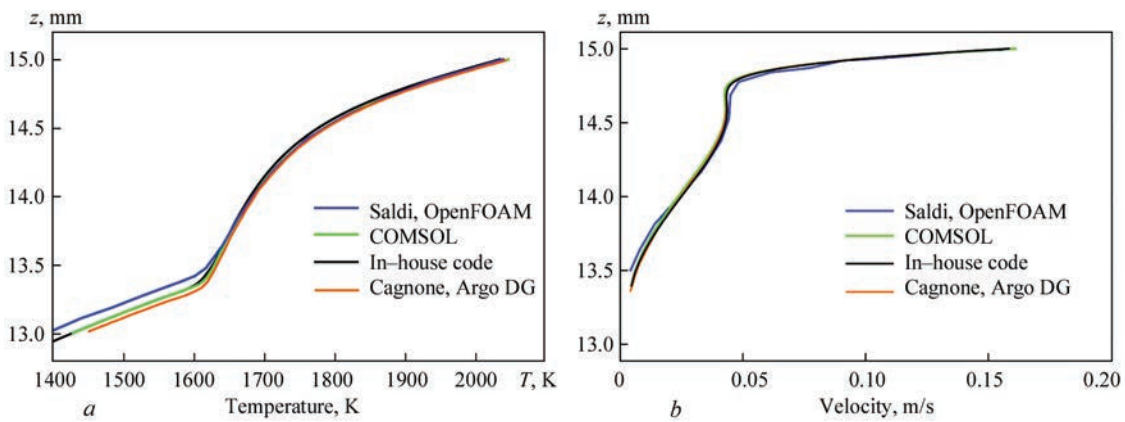

Figure 7. Temperature (*a*) and absolute velocity (*b*) distributions in section r = 1 mm at t = 5 s

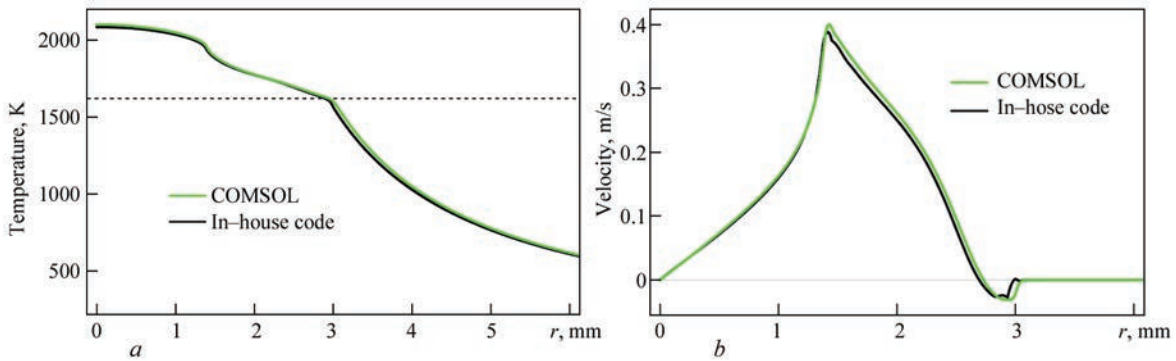

Figure 8. Temperature (*a*) and velocity (*b*) distributions along free surface at t = 5 s

Adaptive FE mesh with gradually increasing linear element dimension from 75 μm (in weld pool region) to 1.35 mm (on the periphery of computational region) was employed (Figure 5). We carried out calculations separately by means of two software tools: commercial software COMSOL Multiphysics and in-hose FE code. We fulfilled comparative analysis of calculated results at t = 5 s. Comparisons of the melt front shapes, velocity and temperature distributions along line r = 1 mm and on weld pool free surface are presented on Figure 6–8 respectively. Slight difference between our results and those obtained in work [13] for melt front position is observed (Figure 6), whereas in the melt region all the calculated results agree well with each other. Flow pattern in the weld pool consists of clockwise vortex in the meridional plane. Velocity in the melt achieves maximum value of 0.38 m/s. Increasing of sulfur content in the metal results in enlargement of the temperature interval where $\gamma > 0$ (Figure 3), which in turn leads to appearance of anticlockwise vortex on the weld pool periphery under the influence of inward shear stress. Such changes in the flow structure give rise to penetration growth. This phenomenon is well studied and is widely reported in literature [6, 7, 1, 13].

Summary

Two test problems dealing with thermocapillary convection were solved separately by means of commercial software COMSOL Multiphysics and in-hose FE code. Comparison of the calculated results with those published earlier was carried out. Good agreement between results obtained with benchmark solutions is observed. Thus, it can be concluded that FE codes in use can successfully be applied for numerical analysis of multiphysics phenomena in the weld pool.

1. Kou, S. (2002) *Welding metallurgy.* New Jersey, John Wiley&Sons.
2. Messler, Jr., Robert, W. (2008) *Principles of welding: Processes, physics, chemistry, and metallurgy.* New Jersey, John Wiley&Sons.
3. Limmaneevichitr, C., Kou, S. (2000) Visualization of Marangoni convection in simulated weld pools. *Welding J.*, 79(**5**), 126–135.
4. Tsai, M. C., Kou, S. (1989) Marangoni convection in weld pools with a free surface. *Int. J. for Numerical Methods in Fluids*, 9(**12**), 1503–1516.
5. Sahoo, P., Debroy, T., McNallan, M. J. (1988) Surface tension of binary metal–surface active solute systems under conditions relevant to welding metallurgy. *Metallurgical Transact.*, *B*, 19(**3**), 483–491.
6. Heiple, C.R. (1982) Mechanism for minor element effect on GTA fusion zone geometry. *Welding J.*, 61(**4**), 97–102.
7. Pitscheneder, W. et al. (1996) Role of sulfur and processing variables on the temporal evolution of weld pool geometry during multikilowatt laser beam welding of steels. *Ibid.*, 75(**3**), 71–80.
8. Kou, S., Sun, D.K. (1985) Fluid flow and weld penetration in stationary arc welds. *Metallurgical Transact.*, *A* 16, **1**, 203–213.
9. Demchenko, V. F., Krivtsun, I.V., Krikent, I.V., Shuba, I.V. (2017). Force interaction of arc current with self-magnetic field. *The Paton Welding J.*, **3**, 15–24. https://doi.org/10.15407/as2017.03.03
10. Brent, A.D., Vaughan R. Voller, K.T.J. Reid (1988) Enthalpy-porosity technique for modeling convection-diffusion phase change: Application to the melting of a pure metal. *Numerical Heat Transfer*, *Pt A: Applications*, 13(**3**), 297–318.
11. Zienkiewicz, O.C., Taylor, R.L. (2000) *The finite element method*. Vol. 3: Fluid dynamics. Oxford, Butterworth-Heinemann.
12. Gupalo, Yu P., Ryazantsev. Yu. S. (1988) Thermocapillary motion of a liquid with a free surface with nonlinear dependence of the surface tension on the temperature. *Fluid Dynamics*, 23(**5**), 752–757.
13. Saldi, Z. (2012) *Marangoni driven free surface flows in liquid weld pools.* Ph.D. Thesis, Delft University of Technology.
14. Cagnone, Jean Sébastien, Koen Hillewaert, Nicolas Poletz (2014) A discontinuous Galerkin method for multiphysics welding simulations. *Key Engineering Materials*. **611**. Transact. Tech Publications Ltd.

Received 10.12.2020